UNIVERSITY OF TURKU

Laser beam shaping effects to quality and productivity in Laser powder bed fusion technology

Konetekniikka / Teknillinen tiedekunta

Valtteri Lainio

18.4.2024

Turku

Bachelor's thesis

Author: Valtteri Lainio

Title: Laser beam shaping effects to quality and productivity in laser powder bed fusion technology
Supervisor: Antti Salminen
Number of pages: 26 pages
Date: 18.4.2024

Abstract:

Laser powder bed fusion (BPF-LB/M) process has over 100 process parameters. In this literature review the effects of laser beam shaping to BPF-LB/M are studied beside of main parameters. Considered effects are quality factors and the properties that can be applied to industry. Quality factors considered are microstructure, mechanical properties, and geometrical accuracy. How laser beam shaping effects to high power processing, productivity and build rate has been viewed from industrial point of view. Laser beam modes which are compared are Gaussian, elliptical, Top-hat, donut, and multimode laser. Depending about the literature, the method varies from literature review to experimental approach. Because of the lack of research papers, the laser power, materials, and laser beam mode reported varies from each other. Today there is no good literature review about the laser beam effects compared to quality and productivity because those usually conflicts and needs more research.

Key words: Laser powder bed fusion, additive manufacturing, laser beam shaping, laser beam mode, quality, microstructure, mechanical properties, high power, productivity,

Table of contents

1 Introduction

1.1 Laser basics

Albert Einstein introduced the "stimulated emission", which is used to produce laser radiation. Based on Einstein's theorem the first laser concept was published in 1960 by Arthur Schawlow and Charles Townes. Theodore Maiman made the first laser operate on 16 May 1960 at the Hughes Research laboratory in California. [1]

In laser devices there are pumping source, which generates energy to the active medium, which amplifies light. In active medium atoms have certain energy state. When atom returns to normal energy state the photon is emitted. The laser beam consists of these photons. Photons from the laser device have same frequency, same phase, same sense of polarisation and same direction. [1]

The wavelength λ in laser is decided by the energy difference as the excited species is stimulated to a lower energy level $E = \frac{hc}{\lambda}$, where h is Planck's constant, c is velocity of light. The transition from state E_1 to E_2 results emission of photon. The frequency v_{12} follows equation $v_{12} = \frac{|E_1 - E_2|}{h}$. The laser output power can be controlled with pumping source or active medium. With optical fiber, laser can be transmitted to optical part where the beam can be shaped to match the desired machining properties. Depending on laser, laser can be either single mode or multi-mode laser. The structure of optical fiber is also different in single mode lasers and multi-mode lasers. Beam quality of single mode laser is better than with multi-mode laser. The intensity distribution from single mode laser is Gaussian and from multi-mode laser it is cylindrical top hat. [1]

1.2 Basics of laser powder bed fusion

Metal-additive manufacturing provides manufacturing of parts with very complex and high-resolution geometry. Therefor AM is typically used when normal manufacturing methods are not accurate enough. AM also promises to reduces costs, time, and low energy consumption of production [2] [3]. Parts nearing the end of lifetime can be repaired or refurbished using AM. Broken parts can be rebuild directly to the old leftover piece. Because AM doesn't need a big manufacturing infrastructure these repairs can be made also in remote locations. [4]

In laser-powder bead fusion (BPF-LB/M) process a laser beam works as a heats source and selectively melts the layer of powder already spread on the substrate [5]. This is made straight from the computer-aided design (CAD) model using a “layer by layer” method [6]. In modern BPF-LB/M machines the scanning velocity can reach to 10000 mm/s. By the literature, values are typically around between 220 mm/s and 3000 mm/s [7, p. 718]. The melted powder solidifies, and the platform moves downwards the distance to supply the required thickness of powder to make a new layer. This is repeated and the part is formed into powder matrix. [8]

It has been shown that compared to other manufacturing processes, some metal alloys have much better properties compared to casting and forcing. The typical high cooling rate of BPF-LB/M often results very small grain sizes and therefor provides good mechanical properties [3]. Although small grain size can be achieved, high cooling rates in order of ($10^5 - 10^6 K \cdot s^{-1}$) can be reached. This can lead to metastable phase formation [2] [3]. Because of rapid solidification and complex thermal history there might be micro and macro scale differences in chemistry, which changes functional and structural properties of the part. Residual stress causes big problems in BPF-LB/M. It is strongly involved because of high thermal gradient. In the proses there is also non-uniform expansion and contraction because of the layer-by-layer technique, where melting and solidification is happening in layers several times. [9] [10]

1.2.1 Parameters in laser powder bed fusion

In modern laser powder ped fusion there are over 100 parameters. These parameters can be shared to machine parameters and process parameters. Machine parameters are not generally changed, and process parameters can be modified from build to build. Most typical parameters are laser power, scan velocity, hatch distance, scan strategies and layer thickness. These parameters are optimized to maximize the quality (see section 2) desired for the piece and to increase build rate. [3]

To achieve high quality and productivity the parameter optimization is needed. There are several different methods to select these parameters. One method is Design of Experiments (DOE), where process parameters are systematically changed, and effects are noticed. Another method is Response Surface Methodology (RSM), which uses mathematical methods to predict optimal parameters and optimize those for maximum quality and productivity. Process mapping tracks the best parameters in different phases. Also, AI and ML can also be used to optimize parameters by learning and predicting. Using and combining these models

can provide significant help to optimize parameters comprehensively to achieve high quality and productivity. [8]

1.3 Basics of laser beam shaping

Laser beam is made in optical oscillator, where standing electromagnetic waves are formed. These waves are formed based on the shape of the chamber in oscillator. The longitudinal standing waves are slightly difference angle and the number of those off-axis waves are in relationship to Fresnel number $N = \frac{a^2}{\lambda L}$, where a is radius of output aperture, L is the cavity length and λ is wavelength. These standing waves interfere with each other, forming transverse standing wave. This wave comes out of the chamber as a mode of laser beam. The intensity distribution $P(r, \varphi)$ of a laser beam is calculated from the square of transverse standing wave amplitude $E(r, \varphi)$ as $P(r, \varphi) = E^2(r, \varphi)$ [1]

In optics the focusing lens gathers the rays to the focal plane. In this point the constructive and destructive interference happens. When waves are at opposite phase, those effects each other negatively and destructive interference happens. If waves are in same phase they have positive effect to each other and constructive interference happens. [1]

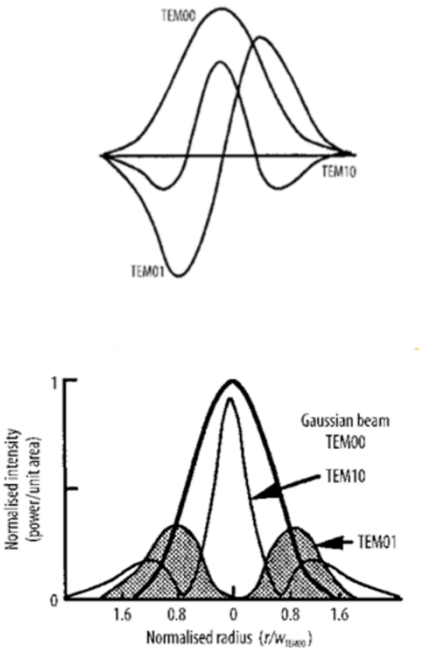

Figure 1. Amplitude variation (top) and intensity distribution (bottom) for various modes. [1]

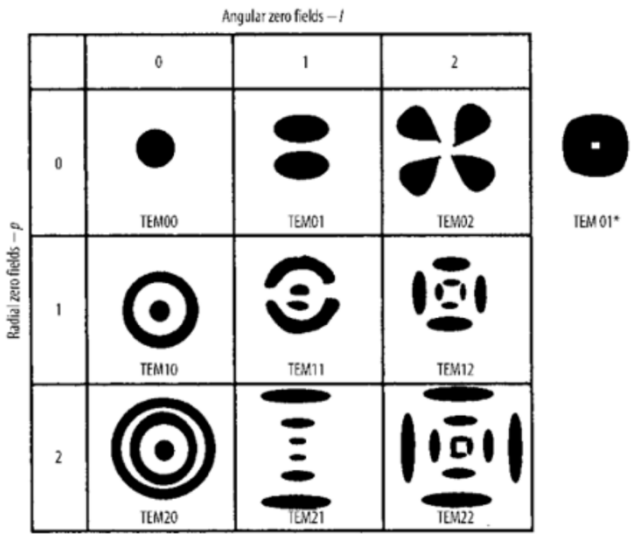

Figure 2. Various mode patterns [1]

These modes are classified as TEM_{plq}. where the number of radial zero fields (p) angular zero field (l) and longitudinal zero field (q). For example the first harmonic distribution (donut) is $TEM_{01^*} = TEM_{01} + TEM_{10}$ and a uniform cylindrical (flat top) is $TEM_{FT} = TEM_{01^*} + TEM_{00}$ [11]. With square beams the distributions are similar but with Hermite polynomials. [1]

With normal Gaussian distribution TEM_{00} the energy flux q$[W/mm^2]$ is calculated as: $q = \frac{P}{\pi r_0^2}\exp\left(-\frac{r^2}{r_0^2}\right)$, where P is laser beam power [W] and r_0 is the radius circle [mm]. The energy flus q inside the beam spot radius r_0 can be calculated as a function of radius r: $q = \frac{P}{\pi r_0^2}\frac{1}{\sqrt{1-r^2/r_0^2}}$. With the cylindrical flat-top thermal distribution the beam boundary (r=r_0) is hard to obtain because of the discontinuity. The TEM_{01^*} is seemed to be reasonable compromise. When the laser hits to the powder layer, the temperature rice over the beam circle is: $T_0 = \frac{P}{4\lambda r_0}$, where λ $[W/mm \cdot K]$ is material thermal conductivity. The radiation is absorbed to the powder and melts it with its energy. The heat transfer mechanism in the part is conduction. [12].

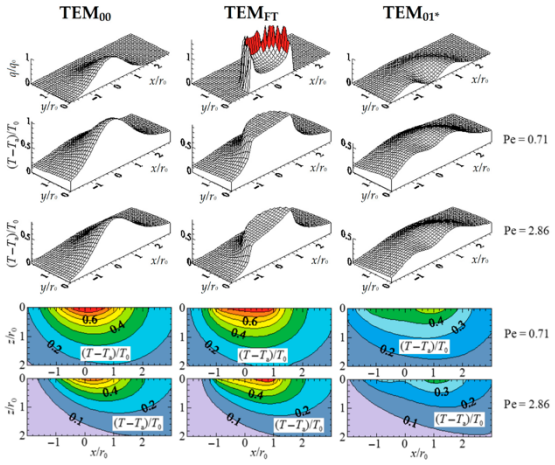

Figure 3. first row: Absorbed laser energy q over target surface. second and third rows: Temperature T over target surface. fourth and fifth rows: Temperature T over vertical plane. [11]

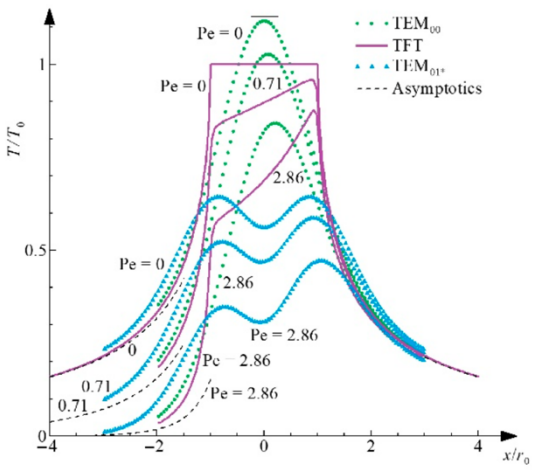

Figure 4. Temperature distributions with several scanning speeds, which are indicated with Péclet number. [11]

2 Laser beam shaping effect to quality factors

In BPF-LB/M the laser scans very fast at the powder surface. A problem of overheating and inversely lack of processing temperature for the scanning laser can be solved by finding the ideal power density distribution. The main solution still depends about the scanning velocity and its direction. The effect of scanning direction to the absorbed energy flux shows that the laser beam profile would be asymmetric. [11]

In BPF-LB/M technology the final part quality can be evaluate in the following main categories, microstructure, mechanical properties, porosity, surface roughness and residual stress. With these factors we can determine the outcome of a BPF-LB/M product and ensure the reliability, functionality, and safety of printed part. Heat input determines the temperature gradient in the powder, influencing the overall melting behaviour. That effects to produced material characteristic such as density, morphology, surface roughness, mechanical properties, and residual stress. Optimizing the processing parameters to achieve one or several quality parameters and increase productivity is difficult because these parameters usually conflicts. Papers that would contain information of BPF-LB/M productivity and part quality is not yet found in the literature. [8]

2.1 Microstructure

2.1.1 Density and porosity

In AM- community there is lot of research about the porosity issues. Specially the relationship between laser power and scan velocity is studied quite extensively. Porosity is mainly causes by too high laser power, which is known as keyhole porosity. Keyhole is a hole formed in the material, which brings heat to the material. If too much power is used it becomes unstable and porosity increases. Pores are formed due to collapse of unstable keyhole, which leads air to be trapped inside molten pool until it is solidified. Keyhole porosity can be avoided by reducing power density or increasing scan velocity. It is important to be able to control melt pool solidification and optimize parameters so that solidification process is delayed [13]. [3]

The lack of fusion porosity is noticeable when laser power is not high enough compared to the volume to be digested. The pores caused by Incomplete melting usually looks thin and non-spherical [14]. This can be avoided with defining the ratio between melt pool depth and layer thickness. Complicated way is calculation of fluid dynamics in melt pool [2]. Another way is

to stimulate overlapping semi-circles or semi-ovals. In this process the analyse of layer thickness and hatch distance is very important. [3]

Tenbrock et. al. [16] showed that while using 2kW laser beam the density is higher and surface is flatter with multi-mode fiber laser compared to Gaussian beam. The difference is mainly caused by molten pool behaviour. Using this amount of power the melt pool with Gaussian beam is usually keyhole mode. With too much power, key hole mode can be complex and violent because of the metal vapor pressure, surface tension and melt gravity [15]. With multi-mode laser beam, the molten pool mode is conduction mode, and the molten pool is more stable. Therefore it enables to create relatively flat surface and dens parts. [16]

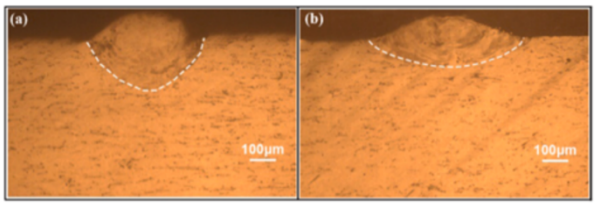

Figure 5. OM cross-section images of single track built. (a) Gaussian beam (b) multi-mode beam. [28]

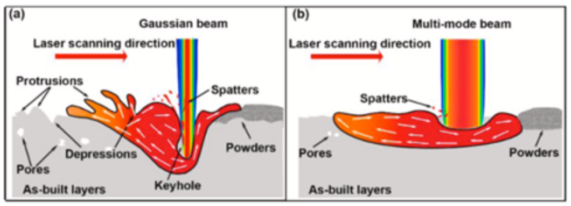

Figure 6. Illustrated images of melt pool behaviour and its effects to density and surface roughness. (a) effect of Gaussian beam (b) effect of multi-mode laser beam. [28]

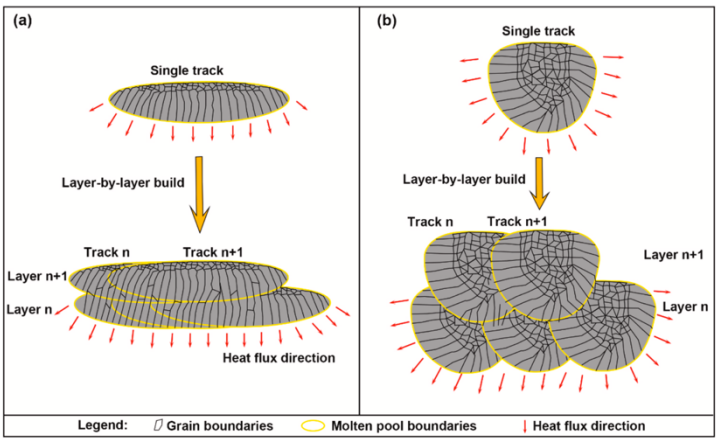

Figure 7. Illustrated effects of (a) multi-mode laser beam (b) Gaussian laser beam, to grain boundaries, molten pool boundaries and heat flux direction in HP-BPF-LB/M. [28]

King et. al. [17] developed an analytical solution for the threshold between conduction and keyhole modes. The threshold is related to laser power P and velocity V. As P and $V^{-1/2}$ respectively, the transformation from conduction mode to keyhole mode occurs. This shows that decreasing laser power has greater effect to eliminate keyhole porosity than increase of scan velocity. Cunningham et al [15] showed that the energy density do not precisely correlate

with the melt pool shape. Because of that it is possible that the keyhole porosity vapors may be generated before difference in melt pool shape is noticed.

Relatively high laser power is commonly used to produce parts with low porosity, higher density and higher productivity [18]. On the other hand, using too much power can cause vaporization and increase porosity and residual stress. In final part this can cause differences in geometry as curling. Using low laser power, the final part has better dimensional accuracy. This also reduces densification and increases the risk of layer delamination [19]. With decreasing of laser power on the second scan of 40% caused improve in mechanical properties. Also Montero Sistiaga et al [20] noticed that using high power lasers increased productivity but also causes coarser microstructure and reduced parts mechanical properties as yield stress and hardness.

The total porosity is influenced by the Volumetric Energy Density (VED). The VED Shows the input energy by a unit volume $VED = \frac{P}{l \cdot h \cdot v_s} [\frac{J}{mm^3}]$. Low VED can lead to lack of fusion porosity as unfused powder between layers. With increased VED the porosity can be improved because of better flow of molten material. When VED is too high it can lead to keyhole porosity. Eliasu et. al. [21] worked with AISI316L demonstrates the effect of VED to porosity and density in (figure 8). In other research this evaluation is also noticed to come to fruition with other alloys too. [22]

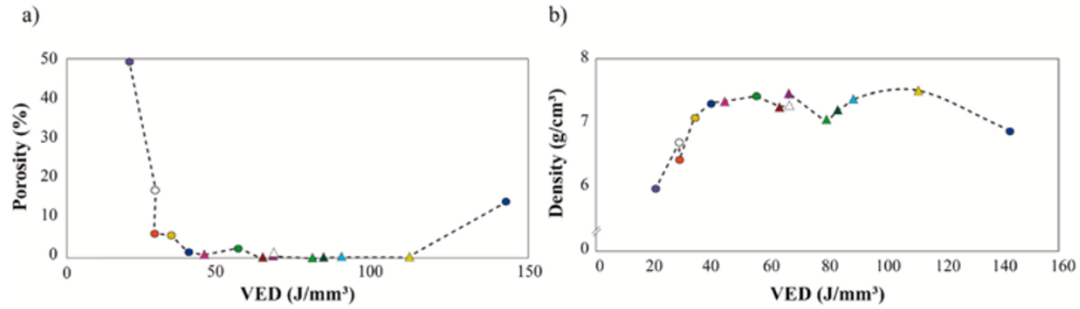

Figure 8. Experimental results of VED versus porosity and density.[21]

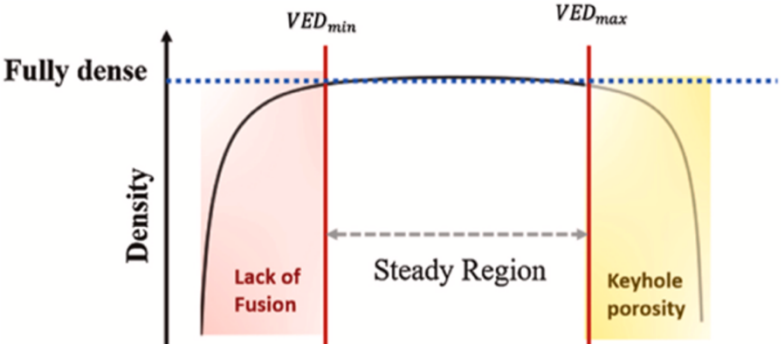

Figure 9. Density as function of VED. [22]

2.1.2 Surface roughness

Surface roughness is significant quality factor in the BPF-LB/M process. The effect of it is important to consider and it is result of a many various parameters. Laser power plays important role in surface quality of final parts. With low laser power there might be high surface roughness and bad dimensional accuracy because of the incomplete melting, especially with thick layer thickness. The incomplete melting can be avoided by increasing laser power and improve the surface roughness and dimensional accuracy. However, with high power and speed this becomes unstable. [23]

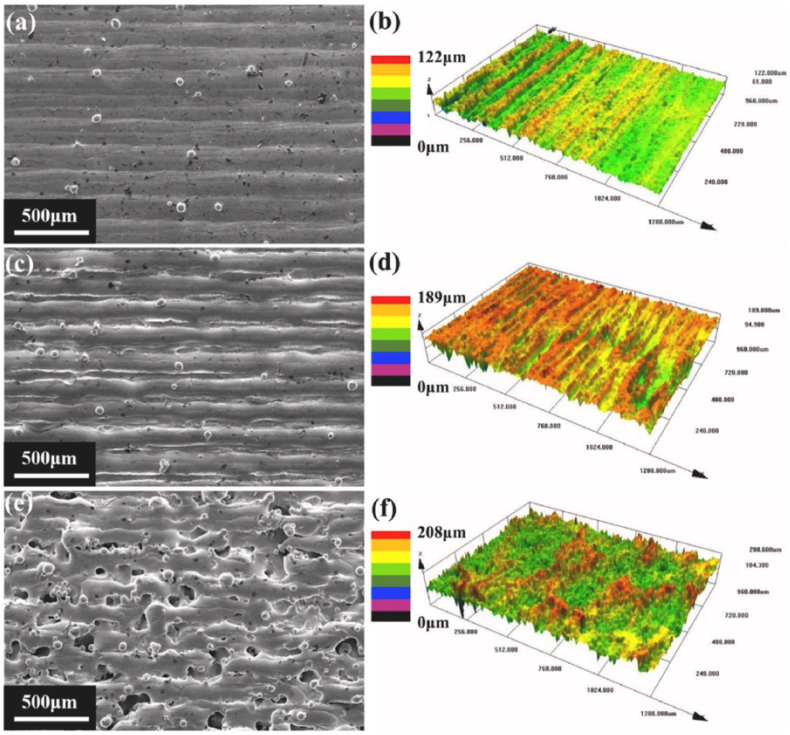

Figure 10. SEM and reconstruction images of top surface. Scan speed 2000mm/s, hach distance 90µm. laser power (a) 150W (b) 250W (c) 350W. [23]

2.1.3 Grain nucleation

In BPF-LB/M the microstructure of a final part is very complex. Typical defects in microstructure of a final part made with BPF-LB/M are micro segregation, undesired texture, coarse columnar grains, and meta-stable phases such as martensite. With increasing or strongly decreasing scan velocity can eliminate micro segregation. Coarse columnar grains and undesired textures can be reduced with decreasing scan velocity or laser power. [8] [3]

AM-technology differs from typical manufacturing methods with it high and localized heating. Melting and solidification directionally from fusion boundary causes high thermal gradient (G) and solidification growth rates (R). This is typically not favourable to achieve equiaxed grain nucleation, which requires low G/R values. Coarse columnar grains can be hundreds of micros long in direction of build direction and continues epitaxially through successive layers. This leads to anisotropic mechanical properties, and it can cause solidification cracking with sensitive alloys. For example, with AISI 316 L stainless steel, the substructure transitions from planar to cellular or cellular-dendritic from fusion boundary to the top of the melt pool as the G/R decreases [24]. [25]

It has shown that using elliptical shape laser beam in place of traditional Gaussian beam there is changes in microstructure of laser melted tracks [24]. With some materials the elliptical beam can increase the volume fraction of equiaxed grains. With test of AISI 316 L stainless steel cubes were made with Gaussian beam and elliptical beam with following parameters. Power in range of 150-350W, energy density in range of 80-260j/mm^3, layer thickness 50µm and hatch distance 100µm. When using the same energy density, the elliptical test cube had smaller vertical spacing between fusion boundaries. In examination pore distribution didn't vary in build direction (figure 11). [25]

With AISI 316 L, using laser power 250W and energy density 140j/mm^3 was made single track test and it was shown that elliptical beam formed much smaller equiaxed grains than Gaussian beam. These parameters were used to build cubes and as a result was shown that the grain size difference wasn't that big with 3 dimensional parts but with elliptical beam the amount of small grains was approximately twice bigger per unit area. These small grains are formed epitaxially from remelted grains through previous layer (figure 12 a) or formed in melt ahead of columnar front on a later phase of solidification (figure 12 b). Grain nucleation in later solidification happens when thermal gradient (G) is relatively low and solidification growth rates (R) is high. [26]

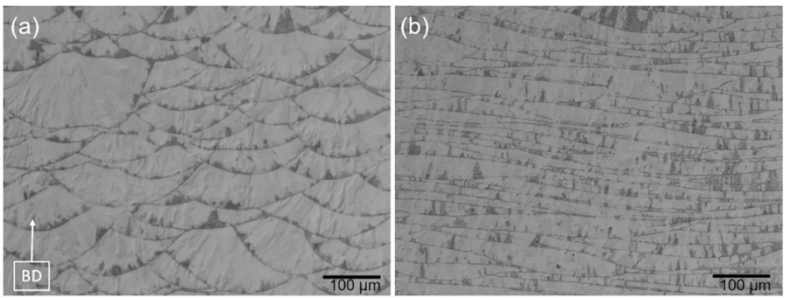

Figure 11. Microstructural cross section images of built cubes with laser power P 250W and Q 140J/mm³. Build direction is indicated with arrow. (a) Gaussian beam sample (b) Elliptical beam sample. No cross-hatching was used. [25]

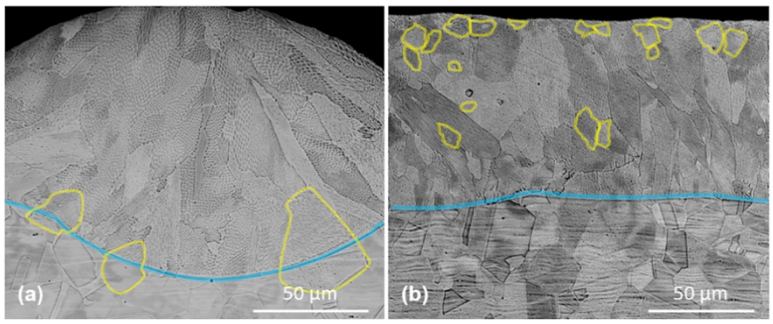

Figure 12. Example picture of SEM micrographs of single track deposited onto AISI 316 L stainless steel with 50µm layer thickness. (a) equiaxed grain (yellow), fusion boundary (blue). (b) equiaxed grains that can be observed in the middle and top of the melt track. [25]

2.2 Mechanical properties

In BPF-LB/M it is possible to create high-strength parts that have even better mechanical properties than with common manufacturing methods. Reason for good mechanical properties of BPF-LB/M parts are finer grain size, cellular microstructure, well distributed nano-sized precipitates, and the supersaturated solid solution obtained with rapid solidification [27]. Also, the part density is one main factor that correlates directly to mechanical properties. With reducing the part porosity to <1% we can achieve favourable mechanical properties. [8]

2.2.1 Weak zone phenomena of molten tracks

The difference in molten tracks in multi-mode laser beam and Gaussian beam effects to the tensile stress. The cellular areas, which are formed to the edges of molten tracks can act as weak zones during the tensile test. Liu et al. [28] noticed that the tracks molten with Gaussian beam has more weak zone facing directly to tensile load than with multi-mode beam molten track (figure 13). This has negative effect to the Gaussian sample tensile properties.

Coarsened cellular areas (figure 14 c, d) are only observed on the fracture surface of the Gaussian sample and it supports the phenomena of weak zones facing directly to tensile load.

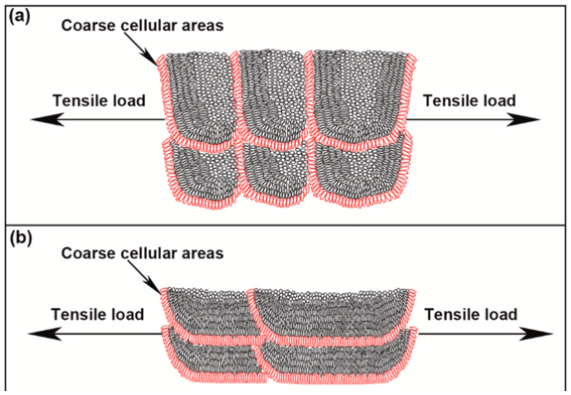

Figure 13. Illustrated pictures of molten track morphologies. (a) Gaussian beam (b) multi-mode beam. [28]

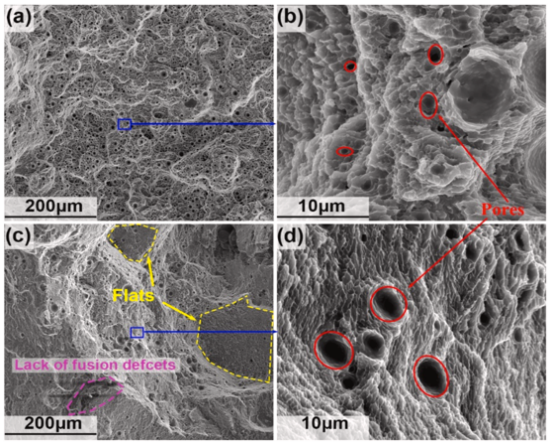

Figure 14. Facture morphologies of typical HP-BPF-LB/M AlSI10mg sample. (a) multi-mode beam (b) Gaussian beam. blue box area shown on right. [28]

2.3 Residual stress

In AM-processes such as BPF-LB/M there is one significant difficulty which is residual stress, it can reach up to 500MPa [29]. That can cause bending, deformations, cracking, and delamination in the part. The residual stress is divided into the part such that tensile stress is typically in top and bottom of the part. In the middle of part there is a large zone of intermediate compressive stress [30].

To reduce residual stress in BPF-LB/M there are several proposed methods. The methods are for example reducing scan velocity, preheating the built platform, use sacrificial support structures to minimize part deformations [3]. These can reduce the residual stress in part and prevent part failure. However the material properties, process parameters and geometry are in significant role with residual stress and with the durability of the part. [8]

3 Laser beam shaping in industry

BPF-LB/M is typically used when the produced part is small, because of the process long build time. BPF-LB/M can produce very complex parts with high quality and with minimum material losses. To achieve this goal is not easy. Especially the balance between quality and productivity has been significant challenge. Those can be achieved by adopting BPF-LB/M with optimized parameters. Now days industry mainly uses continuous wave lasers (CW) in BPF-LB/M to ensure the efficiency. Also review papers about the relationship of productivity and quality in BPF-LB/M is not yet available in literature. [8]

3.1 High power

Today in industry the BPF-LB/M machines typically uses lasers with quite low powers (<500W). That causes low build rate (5-20cm^3/h), which correlates also to long processing cycles and high manufacturing costs [31]. To increase productivity, it has been recently proposed of (≥1kW) high power laser powder bed fusion (HP-BPF-LB/M). For example, it has been applied for fast production of AlSi10Mg aluminium alloy, 300M high strength steel, Hastelloy X nickel-based alloy and 316L stainless steel. With the HP-BPF-LB/M the build rate can achieve up to 103-116cm^3/h, which is almost 5-20 times faster than typical industry laser. [28]

Montero-Sistiaga et al. [20] examined the difference between 1kW top-hat laser beam and 400W Gaussian laser beam with Hastelloy X alloy. The result was found that the density of top-hat laser beam was lower than Gaussian sample. Sow et al. [32] examined the difference of 1kW multi-mode fiber laser and 200W Gaussian laser with IN625 alloy. The result was found that the multi-mode laser can prevent the powder spatters and vaporization effectively. That's why the surface roughness is lower with multi-mode lasers than Gaussian lasers. With multi-mode lasers beam, melt pools during this like of process should be controlled by the conduction mechanism. And with Gaussian laser beam the melt pool should be controlled with the keyhole formation mechanism. [17]

3.1.1 Effects of laser beam shaping to melt pool formation in high powers

In different laser modes the laser power density q can be calculated as $q = \frac{P}{\pi * r^2}$, where the p is laser power and r is the laser beam radius. With Gaussian beam there is higher power density, which causes relatively high temperature in the melt pool. This generally generates

lower surface tension gradient in melt pool, which is the main force to resist formation of keyhole [33] [34]. Because of this it is much easier to reach keyhole mode with Gaussian beam laser.

The threshold conditions to transition from conductivity mode to keyhole mode during BPF-LB/M is developed by King et. al. [17]. In the model the higher normalized enthalpy $\Delta H/hs$ correlates to easier keyhole mode formation. This is calculated as $\frac{\Delta H}{hs} = \frac{AP}{h_s\sqrt{\pi D v \sigma^3}}$, where ΔH is the specific enthalpy, hs is the enthalpy at melting, A is laser absorption coefficient, D is thermal diffusivity, v is scanning velocity. If this is done with both Gaussian beam and multimode beam we can calculate the ratio for those two values k, which tells us how much effectively the laser beam is forming the keyhole mode compared to other.

$k = \frac{(\Delta H/hs)_1}{(\Delta H/hs)_2} = \frac{\sqrt{\sigma^3{}_2}}{\sqrt{\sigma^3{}_1}}$, where $(\Delta H/hs)_1$ and $(\Delta H/hs)_2$ is normalized enthalpy for gaussian and multimode lasers. $\sigma^3{}_1$ and $\sigma^3{}_2$ are the diameters of laser beams.

3.1.2 Effects of laser beam shaping to density in high powers

Comparing the multi-mode fiber laser beam and Gaussian beam to increased VED and the effect of that to relative density. The material used in this exam was AlSi 10 mg. When increasing VED, the relative density of multi-mode laser beam sample first increases and then remains same. From (figure 16 a) multi-mode sample with VED only less than $50j/mm^3$ the relative density is already higher than 99.5%. While Gaussian sample the relative density first increases by increase of VED and then decreases by increased VED. From (figure 16 b), Gaussian mode sample highest relative density is just 95.8 $\pm$ 0.2% at the VED value of $50j/mm^3$. In HP-BPF-LB/M overall densification degree for multi-mode beam is better than Gaussian beam when using 2kW laser beam. Because 2kW is very high power the effects are different in lower powers. [28]

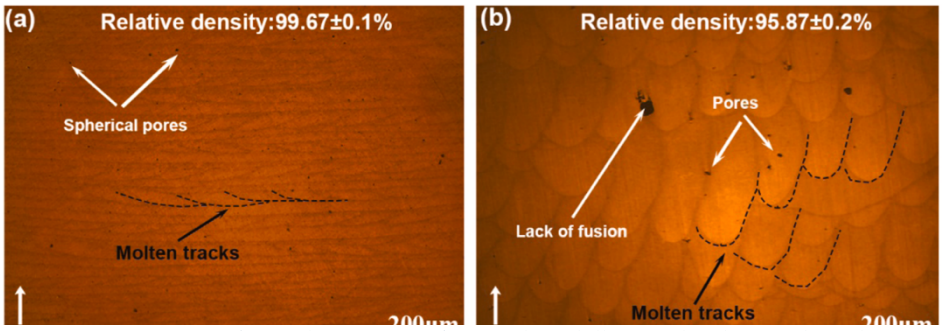

Figure 15. OM images of typical HP-BPF-LB/M sample and illustrated molten tracks and pores. (a) multi-mode sample (b) Gaussian sample. [28]

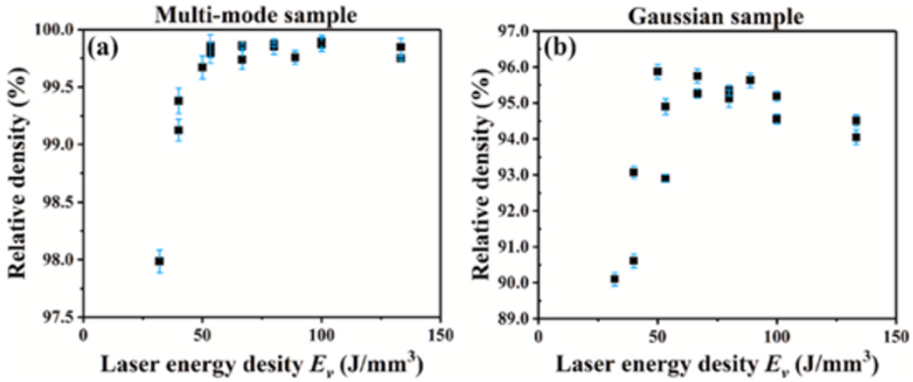

Figure 16. In HP-BPF-LB/M samples relative density as energy density function (VED). (a) multi-mode beam laser sample (b) Gaussian beam sample. [28]

3.1.3 Effects of laser beam shaping to grain nucleation in high powers

Grain nucleation in solidification microstructure varies with laser beam mode. With multi-mode fiber lasers beam the grains have been observed as columnar grains along the build direction. Those columnar grains can be hundreds of micros long and the crystallographic orientation for most of them is <100>. With Gaussian beam the microstructure is a mixture of short columnar grains and equiaxed grains. With Gaussian beam the crystallographic orientation is multifarious, which leads to weaker texture. With multi-mode lasers beam the tensile strength and elongation are much better than with Gaussian beam. The difference in these solidification microstructures should be related to molten track morphology differences between multi-mode laser and Gaussian laser. [28]

3.1.4 Effects of laser beam shaping to mechanical properties in high powers

With high power laser powder bed fusion (HP-BPF-LB/M) produced AlSi10mg sample. Tensile properties such as ultimate tensile stress (UTS), yield strength (YS) and elongation (EL) are shown in the (figure 17). In comparison with multi-mode fiber laser beam and Gaussian beam the effects of multi-mode laser beam have better result in (UTS), (YS) and (EL). Gaussian beam values are 379.7 $\pm$ 21.0MPa, 250.0 $\pm$ 5.7MPa and 4.3 $\pm$ 0.2%. Multi-mode laser values are 444.7 $\pm$ 5.1MPa, 262.3 $\pm$ 1.1MPa and 8.2 $\pm$ 1.6%. [35]

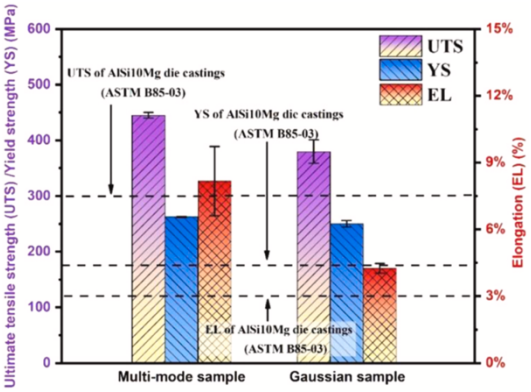

Figure 17. At HP-BPF-LB/M tensile properties of AlSI10Mg sample with multi-mode laser and Gaussian beam. [28]

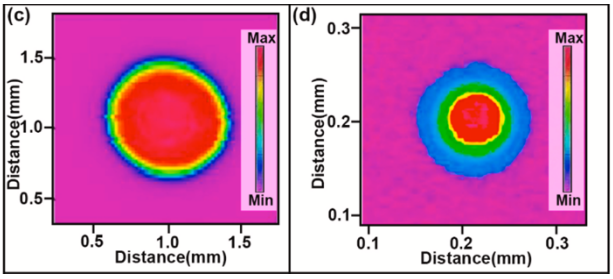

Figure 18. Energy distributions of (a) multi-mode laser beam (b) Gaussian laser beam. [28]

3.2 Productivity

Compared to traditional manufacturing techniques BPF-LB/M suffers relatively low efficiency, which leads to higher manufacturing costs. (Figure 19) shows the balance of quality and productivity. To produce good quality parts BPF-LB/M significantly limits the production time. [8]

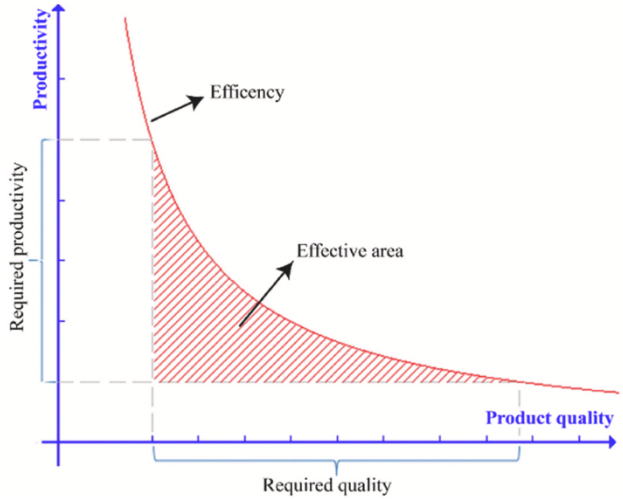

Figure 19. Basic relationship principle of BPF-LB/M process quality and productivity. [36]

3.2.1 VED method to achieve wanted properties with minimum energy.

To improve build speed the VED model is good tool to determine the minimum energy consumption to achieve adequate material fusion for wanted properties. When it is selected the fastest combination of laser power, scan velocity and hatch distance corresponds the maximise productivity for certain machine. In VED equation the maximum BR value

corresponds to minimum VED value with given laser power. With this method we can identify the parameter combinations while maintaining the increased productivity, desirable density, and porosity. Eliasu et al [21] worked with AISI316L demonstrates the effect of VED to porosity and density in (figure 8). [22]

3.2.2 Production time

Build time T_{bld} of a part can be calculated with equation $T_{bld} = T_d +, T_r + T_s$, where T_d is delay time, T_r is recoating time and T_s is scanning time. Delay time includes platform moving to next level. Recoating time is the time that takes to spread new layer of powder to platform. Scanning time includes the time to scan each layer.

productivity $PR = \frac{V_p}{T_p} [\frac{cm^3}{h}]$, where V_p is produced volume and T_p is total processing time.

$T_p = T_{pre} + T_{bld} + T_{post}$, where T_{pre} is prew-processing time, T_{post} is post-processing time.

The T_{pre} includes for example machine setup and CAD model loading. T_{bld} is the build time needed to build the part, which can be varied with machine parameters. T_{post} includes for example support structure removal, powder removal and heat treatment. [8]

4 Future

4.1 The future of AM

BPF-LB/M properties can be difficult to optimize between quality and productivity. It is also desired to change process parameters during process to improve melt pool intensity and part quality. HO Yeung et al [37] proposed to control laser power during the process with algorithm, which is based to the geometric conductance factor (GCF).

With use of AI and machine learning can be used as parameter optimization in real time. This leads higher productivity and part quality when it is possible to focus to specific part properties [38]. In future the research of parameter optimization in BPF-LB/M and also in laser beam shaping is crucial to achieve increase of productivity and to get maximum effort from laser powder bead fusion technology. [8]

In future it is possible to use AM-technologies as a platform for new high-performance alloys because of a powder and layer by layer method. It is also possible to create graded structures if part needs different properties to different places. AM-technologies provides users to create and design their own materials. [3]

4.2 The future of laser beam shaping

The laser beam shaping in real time is rising trend which enables a lot. There are different methods to change beam shape during the process and several companies that make this kind of products. For example, Cailabs produces all kind of optical hardware to aerospace, industrial laser processing and optical fiber networks. For AM and specifically for BPF-LB/M they provide Canunda-HP module with multiple beam mode shapes and fast post-by function to change it in high powers. With their data based on laser beam shaping they promises (x3.3) increase of scan velocity, possibility to print new materials with removing hot-cracking and increase of density. The module can operate with all types of wave lasers and wavelengths from green laser to CO2 lasers. [https://www.cailabs.com]

5 Discussion

Effects of laser beam shaping varies with other process parameters. Main parameters should be set at first and then we can consider shaping the laser beam. It is important to identify desired properties of the part and shape the beam accordingly. The biggest effect of shaping beam to wider energy distribution focus to microstructure and specially to density and grain nucleation positively. With microstructural improvement, mechanical properties are improved. Based on literature it looks like that better distributions than Gaussian are cylindrical top-hat and elliptical. Those beam modes work pretty good with wide power range and improves microstructural and mechanical properties of the part. With wider intensity, high power processing becomes more stable, enabling higher productivity while maintaining the quality.

6 Conclusion

With laser beam shaping we can effect to quality properties of the part, productivity and indirect costs of laser powder bead fusion process. With VED model we can achieve wanted properties with minimum energy. Maximum build rate corresponds to minimum VED value with given laser power. With this method we can identify the best parameter combinations while maintaining the increased productivity, desirable density, and porosity.

A problem of overheating and lack of processing temperature for the scanning laser can be solved with finding the ideal power density distribution. When changing the intensity of the laser it is always important to notice the keyhole and lack of fusion porosity. With higher power and Gaussian beam, melt pool needs to be considered as keyhole mode melt pool. When using lower power and wider power distribution, melt pool needs to be considered as conduction mode melt pool. Decreasing laser power has greater effect to eliminate keyhole porosity than increase of scan velocity.

With the HP-BPF-LB/M the build rate can achieve up to 103-116cm^3/h, which is almost 5-20 times faster than typical industry laser. While using 2kW laser beam the densification degree is higher and surface is flatter with multi-mode fiber laser compared to Gaussian beam. The difference is mainly caused by molten bool behaviour. In HP-BPF-LB/M increase of VED first increased relative density of multi-mode laser sample and then it remained same. With Gaussian beam the increase of VED first increased the relative density and then it decreased. Overall densification degree for multi-mode fiber laser beam is better than Gaussian beam when using 2kW laser beam. It has shown that when using 1kW top-hat beam and 400W Gaussian beam the density of Hastelloy X alloy was lower with top-hat laser. On the other hand, with IN625 alloy, using 1kW multi-mode beam and 200W Gaussian beam the multi-mode beam prevented powder spatters, vaporization, and surface roughness.

Usual defects in BPF-LB/M printed part microstructure are: microsegregation, undesired texture, coarse columnar grains, and meta-stable phases. In BPF-LB/M process are high thermal gradient (G) and solidification growth rates (R), which is typically not favourable to achieve equiaxed grain nucleation, which requires low G/R values. Benefits in BPF-LB/M printed part mechanical properties are caused by finer grain size, cellural microstructure, well distributed nano-sized precipitates and the supersaturated solid solution obtained with rapid solidification (low G/R value). When comparing the difference of elliptical shape laser beam

to Gaussian beam it has shown that in single track test the elliptical beam formed much smaller equiaxed grains than Gaussian beam. With 3-dimensional test the number of small grains was approximately twice bigger per unit area with elliptical beam. In HP-BPF-LB/M multi-mode fiber laser beam forms columnar grains along the build direction. With Gaussian beam, microstructure is mixture of short columnar grains and equiaxed grains. Comparing crystallographic orientation Gaussian beam has multifarious orientation and multi-mode beam has <100>. Because of these differences Gaussian beam has weaker mechanical properties than multi-mode laser beam.

Mechanical properties are highly dependent about the microstructure of the part. Good mechanical properties are results of finer grain size, cellular microstructure, well distributed nano-sized precipitates, and the supersaturated solid solution obtained with rapid solidification. Also, the part density is one main factor that correlates directly to mechanical properties. With reducing the part porosity to <1% we can achieve favourable mechanical properties. Using HP-BPF-LB/M and AlSi10mg, multi-mode fiber laser beam has better results in ultimate tensile stress (UTS), yield strength (YS) and elongation (EL) than using Gaussian beam. In Gaussian beam molten track there is more weak zone facing directly to tensile load than with multi-mode laser molten track. This effects negatively to Gaussian sample tensile properties.

Now days the dynamic beam shaping is one main trends in the industry. With optic technology combined to AI or machine learning we can optimize parameters in real time and increase quality and productivity of the part.

References

[1] W. M. Steen and J. Mazumder, *Laser Material Processing*. London: Springer London, 2010. doi: 10.1007/978-1-84996-062-5.
[2] T. DebRoy *et al.*, "Additive manufacturing of metallic components – Process, structure and properties," *Prog. Mater. Sci.*, vol. 92, pp. 112–224, Mar. 2018, doi: 10.1016/j.pmatsci.2017.10.001.
[3] J. P. Oliveira, A. D. LaLonde, and J. Ma, "Processing parameters in laser powder bed fusion metal additive manufacturing," *Mater. Des.*, vol. 193, p. 108762, Aug. 2020, doi: 10.1016/j.matdes.2020.108762.
[4] T. A. Rodrigues, V. Duarte, R. M. Miranda, T. G. Santos, and J. P. Oliveira, "Current Status and Perspectives on Wire and Arc Additive Manufacturing (WAAM)," *Materials*, vol. 12, no. 7, Art. no. 7, Jan. 2019, doi: 10.3390/ma12071121.
[5] M. H. Mosallanejad, B. Niroumand, A. Aversa, and A. Saboori, "In-situ alloying in laser-based additive manufacturing processes: A critical review," *J. Alloys Compd.*, vol. 872, p. 159567, Aug. 2021, doi: 10.1016/j.jallcom.2021.159567.
[6] V. Matilainen, H. Piili, A. Salminen, T. Syvänen, and O. Nyrhilä, "Characterization of Process Efficiency Improvement in Laser Additive Manufacturing," *Phys. Procedia*, vol. 56, pp. 317–326, Jan. 2014, doi: 10.1016/j.phpro.2014.08.177.
[7] G. Macoretta, L. Bertini, B. D. Monelli, and F. Berto, "Productivity-oriented SLM process parameters effect on the fatigue strength of Inconel 718," *Int. J. Fatigue*, vol. 168, p. 107384, Mar. 2023, doi: 10.1016/j.ijfatigue.2022.107384.
[8] M. Taghian, M. H. Mosallanejad, E. Lannunziata, G. Del Greco, L. Iuliano, and A. Saboori, "Laser powder bed fusion of metallic components: Latest progress in productivity, quality, and cost perspectives," *J. Mater. Res. Technol.*, vol. 27, pp. 6484–6500, Nov. 2023, doi: 10.1016/j.jmrt.2023.11.049.
[9] B. E. Carroll *et al.*, "Functionally graded material of 304L stainless steel and inconel 625 fabricated by directed energy deposition: Characterization and thermodynamic modeling," *Acta Mater.*, vol. 108, pp. 46–54, Apr. 2016, doi: 10.1016/j.actamat.2016.02.019.
[10] G. Vastola, G. Zhang, Q. X. Pei, and Y.-W. Zhang, "Controlling of residual stress in additive manufacturing of Ti6Al4V by finite element modeling," *Addit. Manuf.*, vol. 12, pp. 231–239, Oct. 2016, doi: 10.1016/j.addma.2016.05.010.
[11] S. N. Grigoriev *et al.*, "Beam Shaping in Laser Powder Bed Fusion: Péclet Number and Dynamic Simulation," *Metals*, vol. 12, no. 5, p. 722, Apr. 2022, doi: 10.3390/met12050722.
[12] A. V. Gusarov, "Radiative transfer, absorption, and reflection by metal powder beds in laser powder-bed processing," *J. Quant. Spectrosc. Radiat. Transf.*, vol. 257, p. 107366, Dec. 2020, doi: 10.1016/j.jqsrt.2020.107366.
[13] A. Matsunawa, "Problems and solutions in deep penetration laser welding," *Sci. Technol. Weld. Join.*, vol. 6, no. 6, pp. 351–354, 2001, doi: 10.1179/stw.2001.6.6.351.
[14] W. J. Sames, F. A. List, S. Pannala, R. R. Dehoff, and S. S. Babu, "The metallurgy and processing science of metal additive manufacturing," *Int. Mater. Rev.*, vol. 61, no. 5, pp. 315–360, Jul. 2016, doi: 10.1080/09506608.2015.1116649.
[15] R. Cunningham *et al.*, "Keyhole threshold and morphology in laser melting revealed by ultrahigh-speed x-ray imaging," *Science*, vol. 363, no. 6429, pp. 849–852, Feb. 2019, doi: 10.1126/science.aav4687.
[16] C. Tenbrock *et al.*, "Influence of keyhole and conduction mode melting for top-hat shaped beam profiles in laser powder bed fusion," *J. Mater. Process. Technol.*, vol. 278, p. 116514, Apr. 2020, doi: 10.1016/j.jmatprotec.2019.116514.
[17] W. E. King *et al.*, "Observation of keyhole-mode laser melting in laser powder-bed fusion additive manufacturing," *J. Mater. Process. Technol.*, vol. 214, no. 12, pp. 2915–2925, Dec. 2014, doi: 10.1016/j.jmatprotec.2014.06.005.
[18] A. Leicht, M. Rashidi, U. Klement, and E. Hryha, "Effect of process parameters on the microstructure, tensile strength and productivity of 316L parts produced by laser powder bed fusion," *Mater. Charact.*, vol. 159, p. 110016, Jan. 2020, doi: 10.1016/j.matchar.2019.110016.
[19] I. $$Tauthor$$ Gibson, *Additive manufacturing technologies*, Third edition. Cham,

Switzerland: Springer, 2021. doi: 10.1007/978-3-030-56127-7.
[20] M. L. Montero-Sistiaga, S. Pourbabak, J. Van Humbeeck, D. Schryvers, and K. Vanmeensel, "Microstructure and mechanical properties of Hastelloy X produced by HP-SLM (high power selective laser melting)," *Mater. Des.*, vol. 165, p. 107598, Mar. 2019, doi: 10.1016/j.matdes.2019.107598.
[21] A. Eliasu, A. Czekanski, and S. Boakye-Yiadom, "Effect of laser powder bed fusion parameters on the microstructural evolution and hardness of 316L stainless steel," *Int. J. Adv. Manuf. Technol.*, vol. 113, no. 9, pp. 2651–2669, Apr. 2021, doi: 10.1007/s00170-021-06818-9.
[22] S. Cacace and Q. Semeraro, "Improvement of SLM Build Rate of A357 alloy by optimizing Fluence," *J. Manuf. Process.*, vol. 66, pp. 115–124, Jun. 2021, doi: 10.1016/j.jmapro.2021.03.043.
[23] C. Guo *et al.*, "Effect of processing parameters on surface roughness, porosity and cracking of as-built IN738LC parts fabricated by laser powder bed fusion," *J. Mater. Process. Technol.*, vol. 285, p. 116788, Nov. 2020, doi: 10.1016/j.jmatprotec.2020.116788.
[24] T. T. Roehling *et al.*, "Modulating laser intensity profile ellipticity for microstructural control during metal additive manufacturing," *Acta Mater.*, vol. 128, pp. 197–206, Apr. 2017, doi: 10.1016/j.actamat.2017.02.025.
[25] T. T. Roehling *et al.*, "Controlling grain nucleation and morphology by laser beam shaping in metal additive manufacturing," *Mater. Des.*, vol. 195, no. C, pp. 109071-, 2020, doi: 10.1016/j.matdes.2020.109071.
[26] M. J. Bermingham, D. H. StJohn, J. Krynen, S. Tedman-Jones, and M. S. Dargusch, "Promoting the columnar to equiaxed transition and grain refinement of titanium alloys during additive manufacturing," *Acta Mater.*, vol. 168, pp. 261–274, Apr. 2019, doi: 10.1016/j.actamat.2019.02.020.
[27] Q. B. Nguyen, D. N. Luu, S. M. L. Nai, Z. Zhu, Z. Chen, and J. Wei, "The role of powder layer thickness on the quality of SLM printed parts," *Arch. Civ. Mech. Eng.*, vol. 18, no. 3, pp. 948–955, Jul. 2018, doi: 10.1016/j.acme.2018.01.015.
[28] M. Liu, K. Wei, X. Yue, G. Huang, J. Deng, and X. Zeng, "High power laser powder bed fusion of AlSi10Mg alloy: Effect of laser beam mode," *J. Alloys Compd.*, vol. 909, pp. 164779-, 2022, doi: 10.1016/j.jallcom.2022.164779.
[29] Z. Sun, X. Tan, S. B. Tor, and W. Y. Yeong, "Selective laser melting of stainless steel 316L with low porosity and high build rates," *Mater. Des.*, vol. 104, pp. 197–204, Aug. 2016, doi: 10.1016/j.matdes.2016.05.035.
[30] A. Ulbricht *et al.*, "Separation of the Formation Mechanisms of Residual Stresses in LPBF 316L," *Metals*, vol. 10, no. 9, Art. no. 9, Sep. 2020, doi: 10.3390/met10091234.
[31] T. DebRoy *et al.*, "Scientific, technological and economic issues in metal printing and their solutions," *Nat. Mater.*, vol. 18, no. 10, pp. 1026–1032, Oct. 2019, doi: 10.1038/s41563-019-0408-2.
[32] M. C. Sow *et al.*, "Influence of beam diameter on Laser Powder Bed Fusion (L-PBF) process," *Addit. Manuf.*, vol. 36, p. 101532, Dec. 2020, doi: 10.1016/j.addma.2020.101532.
[33] C. X. Zhao *et al.*, "The effect of oxygen on transitional Marangoni flow in laser spot welding," *Acta Mater.*, vol. 58, no. 19, pp. 6345–6357, Nov. 2010, doi: 10.1016/j.actamat.2010.07.056.
[34] C. A. Biffi, J. Fiocchi, P. Bassani, and A. Tuissi, "Continuous wave vs pulsed wave laser emission in selective laser melting of AlSi10Mg parts with industrial optimized process parameters: Microstructure and mechanical behaviour," *Addit. Manuf.*, vol. 24, pp. 639–646, Dec. 2018, doi: 10.1016/j.addma.2018.10.021.
[35] Z. H. Xiong, S. L. Liu, S. F. Li, Y. Shi, Y. F. Yang, and R. D. K. Misra, "Role of melt pool boundary condition in determining the mechanical properties of selective laser melting AlSi10Mg alloy," *Mater. Sci. Eng. A*, vol. 740–741, pp. 148–156, Jan. 2019, doi: 10.1016/j.msea.2018.10.083.
[36] A. V. Gusarov *et al.*, "On productivity of laser additive manufacturing," *J. Mater. Process. Technol.*, vol. 261, pp. 213–232, Nov. 2018, doi: 10.1016/j.jmatprotec.2018.05.033.
[37] H. Yeung, B. Lane, and J. Fox, "Part geometry and conduction-based laser power control for powder bed fusion additive manufacturing," *Addit. Manuf.*, vol. 30, p. 100844, Dec. 2019, doi: 10.1016/j.addma.2019.100844.
[38] T. Shi, J. Sun, J. Li, G. Qian, and Y. Hong, "Machine learning based very-high-cycle fatigue life prediction of AlSi10Mg alloy fabricated by selective laser melting," *Int. J. Fatigue*, vol. 171, p.

107585, Jun. 2023, doi: 10.1016/j.ijfatigue.2023.107585.